PHYSICAL REVIEW B VOLUME 61, NUMBER 2 1 JANUARY 2000-II

Theory of spin-resolved Auger-electron spectroscopy of ferromagnetic 3*d*-transition metals

T. Wegner,* M. Potthoff, and W. Nolting
Theoretische Festkörperphysik, Institut für Physik, Humboldt-Universität zu Berlin, Invalidenstraße 110, 10115 Berlin, Germany
(Received 13 April 1999; revised manuscript received 16 September 1999)

Core-valence-valence Auger electron spectra are calculated for a multiband Hubbard model including correlations among valence electrons as well as correlations between core and valence electrons. The interest is focused on the ferromagnetic 3*d*-transition metals. The Auger line shape is calculated from a three-particle Green function. A realistic one-particle input is taken from tight-binding band-structure calculations. Within a diagrammatic approach we can distinguish between the direct correlations among those electrons participating in the Auger process and the indirect correlations in the rest system. The indirect correlations are treated within second-order perturbation theory for the self-energy. The direct correlations are treated using the valence-valence ladder approximation and the first-order perturbation theory with respect to valence-valence and core-valence interactions. The theory is evaluated numerically for ferromagnetic Ni. We discuss the spin-resolved quasiparticle band structure and the Auger spectra and investigate the influence of the core hole.

I. INTRODUCTION

Auger-electron spectroscopy (AES) and the complementary appearance-potential spectroscopy (APS) have become valuable tools for investigating the electronic structure of solids and solid surfaces.[1–8] They represent highly element specific and nondestructive methods with a comparatively simple experimental setup. The Auger line shape from a core-valence-valence (CVV) process yields information on the occupied part of the valence band, while APS provides insight into the unoccupied valence states. However, much effort has been spent on the detailed interpretation of the spectra.

Lander[9] suggested that the spectrum obtained by AES (APS) is given as the self-convolution of the occupied (unoccupied) valence density of states (DOS). On the other hand, Powell[10] discovered the CVV Auger line shape of Ag to behave ''anomalously'' in the sense of Lander's self-convolution model. These anomalous features are by now well known to be caused by correlation effects dominating the electronic properties of various solids. Therefore, AES (APS) seems to be a useful technique to study electron-correlation effects, but it is doubtful whether it is able to compete with one-particle spectroscopies, such as photoemission (inverse photoemission), in deriving the DOS by deconvolution.

In the theoretical treatment of the CVV Auger process, there are mainly two problems. The first one is to take into account the correlation effects. Here one may distinguish between *direct* and *indirect* correlations. The direct correlations describe the correlations of those electrons which participate in the Auger process. They are responsible for the most prominent effects in the Auger line shape as compared to the self-convolution. On the other hand, the indirect correlations among the electrons in the rest system manifest themselves in the quasiparticle density of states (QDOS) as a renormalization of the one-particle DOS.

The second problem is the calculation of the transition-matrix elements for the Auger process as well as the scattering of the outgoing Auger electron (cf. Refs. 11 and 12). These effects will (slightly) modify the bare line shape and may become important for a refined interpretation of experimental data. Within the present paper, however, we set aside this second problem and concentrate on electron-correlation effects in AES from ferromagnetic 3*d*-transition metals.

Within the framework of the single-band Hubbard model, correlation effects can be treated exactly for systems with completely filled or empty bands, as was first shown by Cini and Sawatzky.[13–15] The generalization to the case of degenerate bands was introduced in Ref. 16 and further analyzed in Ref. 17, for example. These results may also be extended to include the core-valence interaction.[18]

Considering the more general case of partially filled bands introduces several complications concerning indirect as well as direct correlations. For the indirect valence-valence correlations there is a number of approximation schemes applicable to a multiband Hubbard model. A method which reproduces the experimentally observed Curie temperature quite well, especially for Ni, is the spectral density approach.[19,20] Other approaches are, for example, the generalization of the single-band modified perturbation theory[21] to the multiband model[22,23] and quantum Monte Carlo simulations[24] in connection with the dynamical mean-field theory.[25] However, these methods suffer from some necessary restrictions concerning the completeness of the Coulomb matrix. This is not the case for the fluctuation exchange[26] and the Hubbard I approximation,[23] for example. For a more detailed discussion on the indirect valence-valence correlations see Ref. 23.

For the treatment of the direct correlations, one has the exact-diagonalization method[27] for small systems and the equation-of-motion method[28,29] with its in general uncontrolled termination of the hierarchy of the equations of motion. Another approximate solution is the valence-valence ladder (VV ladder) approximation[30–34] and its generalization to include the core-valence interaction[35–38] (CVV ladder). In particular one has to account for the broken translational symmetry in the initial state of AES, caused by the presence of the core hole and its screening due to the valence electrons. In the final state this interaction is responsible for the sudden response of the valence electrons due to the destruction of the core hole. In the limit of completely filled or empty bands the ladder approximations recover the above-mentioned exact solution.

Here the interaction strength is taken as the control parameter, which is correct in the weak-coupling regime. We are aware that this method has restrictions for the $3d$-transition metals. However, in this work we prefer a common treatment of one-particle spectroscopies (photoemission and inverse photoemission) and two-particle spectroscopies like AES. To be concrete, we will use the second-order perturbation theory around the Hartree-Fock solution[39–41] for the indirect valence-valence correlations. The direct correlations will be treated by applying two different methods, i.e., the VV ladder approximation and the first-order perturbation theory in the valence-valence and core-valence interactions.

Within this approach it is possible to include a realistic one-particle input taken from tight-binding band-structure calculations. We do not only account for the degeneracy of the $3d$ band but also for the hybridization with the $4s$ and $4p$ states. The theory is formulated and evaluated for a nonorthogonal basis set where the states can be distinguished by the angular momentum quantum number and the cubic harmonic index. This facilitates the interpretation of the resulting spectra. Furthermore, we do not restrict ourselves to correlations among the final-state holes only and include core-hole effects from the very beginning. This implies the necessity for a proper treatment of the initial state where the core-hole screening breaks the translational symmetry. The theory is implemented numerically and evaluated for ferromagnetic Ni.

The paper is organized as follows. In the next section we will introduce the model under consideration. In Sec. III we give the expression for the Auger intensity. Section IV concentrates on the indirect and Sec. V on the direct correlations. Finally, Sec. VI concludes the paper. Some details concerning the nonorthogonal basis set are given in the Appendix.

II. MODEL

The Hamiltonian $H=H_0-\mu N+H_I$ is decomposed into a one-particle part $H_0-\mu N$ and an interaction part H_I. N is the operator for the particle number. The one-particle part describes noninteracting valence and core electrons:

$$H_0-\mu N=\sum_{\substack{i,i',\sigma\\ L,L'}}(t_{ii'}^{LL'}-\mu S_{ii'}^{LL'})c_{iL\sigma}^{\dagger}c_{i'L'\sigma}+\sum_{i,\sigma}(\epsilon_c-\mu)b_{i\sigma}^{\dagger}b_{i\sigma}. \tag{1}$$

The index i refers to lattice sites, σ is the spin index ($\sigma=\uparrow,\downarrow$), and $L=\{l,m\}$ is the orbital index with angular momentum quantum number l and cubic harmonic index m. $c_{iL\sigma}^{\dagger}(c_{iL\sigma})$ denotes the creation (annihilation) operator of a valence electron at the lattice site i with spin σ and orbital index L while $b_{i\sigma}^{\dagger}(b_{i\sigma})$ creates (annihilates) a core electron. The core states are assumed to be nondegenerate and dispersionless with the one-particle energy ϵ_c well below the chemical potential μ. The hopping integrals $t_{ii'}^{LL'}$,

$$\langle iL\sigma|h^{BS}|i'L'\sigma'\rangle=t_{ii'}^{LL'}\,\delta_{\sigma\sigma'} \tag{2}$$

(h^{BS} denotes the Hamiltonian of the tight-binding band-structure calculation) are taken from Ref. 42 as well as the overlap integrals $S_{ii'}^{LL'}$:

$$\langle iL\sigma|i'L'\sigma'\rangle=S_{ii'}^{LL'}\,\delta_{\sigma\sigma'}. \tag{3}$$

$t_{ii'}^{LL'}$ and $S_{ii'}^{LL'}$ refer to a nonorthogonal basis set (see the Appendix). Contrary to an orthonormal basis set (where the overlap matrix is replaced by $\delta_{ii'}\delta_{LL'}$), the basis states under consideration can be characterized by the orbital index $L=\{l,m\}$. The construction operators likewise refer to the nonorthogonal basis and satisfy the following anticommutation rules:

$$[c_{iL\sigma},c_{i'L'\sigma'}]_+=0,$$

$$[c_{iL\sigma},c_{i'L'\sigma'}^{\dagger}]_+=(S^{-1})_{ii'}^{LL'}\,\delta_{\sigma\sigma'}. \tag{4}$$

It should be noted that the action of the creation operator on the vacuum state $c_{iL\sigma}^{\dagger}|0\rangle$, in general, does not yield $|iL\sigma\rangle$ [see Eq. (A5) of the Appendix].

To describe the correlations among the valence electrons (VV) as well as the correlations between valence and core electrons (CV) the interaction consists of two parts

$$H_I=\frac{1}{2}\sum_{\substack{i,\sigma,\sigma',\\ L_1,\dots,L_4}}U_{L_1L_2L_4L_3}c_{iL_1\sigma}^{\dagger}c_{iL_2\sigma'}^{\dagger}c_{iL_3\sigma'}c_{iL_4\sigma}-H_{dc}^{\mathrm{VV}}+\sum_{i,\sigma,\sigma',L}U_L^c n_{iL\sigma}n_{i\sigma'}^c-H_{dc}^{\mathrm{CV}}. \tag{5}$$

Here the occupation number operator for valence electrons is $n_{iL\sigma}=c_{iL\sigma}^{\dagger}c_{iL\sigma}$ and for core electrons $n_{i\sigma}^c=b_{i\sigma}^{\dagger}b_{i\sigma}$. Assuming a strong screening of the Coulomb interaction, the interaction part is taken to be purely local. $U_{L_1L_2L_4L_3}$ are the on-site Coulomb-matrix elements for the valence electrons.

The electronic structure of the $3d$ transition metals may be understood considering mainly two types of electronic orbitals: the $4s$ and $4p$ states which form broad free-electron-like bands. They should be well described by the band-structure calculation. The other group are the well localized $3d$ states which in the solid form relatively narrow bands positioned around the Fermi energy. The localized nature of the $3d$ electrons gives rise to important dynamic $3d$-$3d$ correlation effects which are believed to be responsible, e.g., for the magnetic behavior of the $3d$ transition metals. These correlations may not be adequately taken into account within a mean-field picture. We thus treat them separately.

Exploiting atomic symmetries, one is able to express all remaining Coulomb-matrix elements for the $3d$ electrons in terms of three effective Slater integrals[43,44] (F^0,F^2,F^4) only. These integrals are connected to averaged values for direct terms

$$U=\frac{1}{25}\sum_{L,L'}U_{LL'LL'}=F^0 \tag{6}$$

and exchange interaction terms

$$J=\frac{7}{5}\,\frac{1}{20}\sum_{L\neq L'}U_{LL'L'L}=\frac{F^2+F^4}{14}. \tag{7}$$

For $3d$ elements one has to good accuracy the ratio $F^2/F^4 \approx 0.625$ (Ref. 44), be that of free ions.[43] U and J are treated as free parameters to be fixed by comparison with experimental results (see Sec. IV).

The CV interaction part is necessary to describe the core hole effects in AES. U_L^c in Eq. (5) are the Coulomb-matrix elements between the valence and the core electrons which can be fixed by assuming complete screening of the core hole by the valence electrons (see Sec. IV).

To avoid a double counting of interactions, we subtract the correction $H_{dc}^{\mathrm{VV(CV)}}$ which is to a good approximation the Hartree-Fock part of the respective interaction term.[44]

III. AUGER INTENSITY

The Auger process can be divided into two subprocesses. The first one is the creation of a core hole with spin σ_c at the lattice site i_c by absorbing an x-ray quantum, for example. The second subprocess is the radiationless decay of the core hole via ejecting an Auger electron with spin σ and momentum $\mathbf{k}$. Provided that the lifetime of the core hole is large compared to typical relaxation times of the valence electrons in the presence of the core hole, the two subprocesses become independent from each other[3] (two-step model). This implies the absence of any decay term in the Hamiltonian. Consequently $n^c_{i_c\sigma_c}$ is a good quantum number, $[H,n^c_{i_c\sigma_c}]_-=0$. We can concentrate on the second subprocess. Within the two-step model the initial state for the Auger transition process is the ground state within the subspace $\mathcal{H}^e$ of the Hilbert space $\mathcal{H}$ that is built up by all many-body states with $n^c_{i_c\sigma_c}=0$. To perform thermodynamic averages in practice, one has to take into account this restriction by introducing an additional Lagrange parameter.

The transition process itself is described by the transition operator[35]

$$T_{\mathbf{k}\sigma\sigma_c}=\sum_{L_1,L_2}M^{L_1L_2}_{i_c\mathbf{k}}c^\dagger_{i_cL_1\sigma}c^\dagger_{i_cL_2\sigma_c}b_{i_c\sigma_c}. \tag{8}$$

$\mathbf{k}$ and σ denote the quantum numbers of the Auger electron, σ_c the spin of the core state involved. The (intra-atomic) Auger-matrix elements are given by

$$\begin{aligned}M^{L_1L_2}_{i_c\mathbf{k}}&=\langle i_cL_1,i_cL_2|H_{\mathrm{Coulomb}}|\mathbf{k},i_c\rangle\\&\propto\int\int d^3r_1d^3r_2\overline{\Psi}_{L_1}(\mathbf{r}_1-\mathbf{R}_{i_c})\overline{\Psi}_{L_2}(\mathbf{r}_2-\mathbf{R}_{i_c})\\&\quad\times\frac{1}{|\mathbf{r}_1-\mathbf{r}_2|}\Phi_{\mathbf{k}}(\mathbf{r}_1)\phi(\mathbf{r}_2-\mathbf{R}_{i_c}),\end{aligned} \tag{9}$$

where Ψ is the valence orbital, Φ the one-particle wave function of the Auger electron, and ϕ the core state. The overbar denotes complex conjugation.

Following Ref. 35 we consider the (retarded) three-particle Green function, relevant for AES, which is defined as [with the abbreviation $\mathbf{L}=(L_1,L_2)$ and $\mathbf{L}'=(L_1',L_2')$]

$$G^{(3)}_{\mathbf{k}\sigma\sigma_c}(E)=\langle\langle T^\dagger_{\mathbf{k}\sigma\sigma_c};T_{\mathbf{k}\sigma\sigma_c}\rangle\rangle_E=\sum_{\mathbf{L},\mathbf{L}'}\overline{M}^{\mathbf{L}}_{i_c\mathbf{k}}G^{(3),\mathbf{LL}'}_{i_c\sigma\sigma_c}(E)M^{\mathbf{L}'}_{i_c\mathbf{k}}, \tag{10}$$

with

$$G^{(3),\mathbf{LL}'}_{i_c\sigma\sigma_c}(E)=\langle\langle b^\dagger_{i_c\sigma_c}c_{i_cL_2\sigma_c}c_{i_cL_1\sigma};c^\dagger_{i_cL_1'\sigma}c^\dagger_{i_cL_2'\sigma_c}b_{i_c\sigma_c}\rangle\rangle_E. \tag{11}$$

$\langle\langle\cdot;\cdot\rangle\rangle_E$ refers to Zubarev Green functions.[45,46] The AES intensity is then mainly given by the three-particle spectral-density $A^{(3)}_{\mathbf{k}\sigma\sigma_c}(E)=-(1/\pi)\mathrm{Im}\,G^{(3)}_{\mathbf{k}\sigma\sigma_c}(E)$:

$$I_{\mathbf{k}\sigma\sigma_c}(E+\epsilon_c-\mu)\propto\delta(E-E(\mathbf{k}))A^{(3)}_{\mathbf{k}\sigma\sigma_c}(E). \tag{12}$$

Here $E(\mathbf{k})$ is the dispersion of the Auger electron.

In general the three-particle Green function will be a (complicated) functional of one-particle Green functions. This functional represents the direct correlations. In the following we concentrate on the indirect correlations first, i.e., on the determination of the relevant one-particle Green functions.

IV. INDIRECT CORRELATIONS

A. Valence-band interaction

We consider the (retarded) one-particle valence-band Green function $\langle\langle c_{iL\sigma};c^\dagger_{i'L'\sigma}\rangle\rangle_E$. Using a matrix notation with respect to the orbital index $L=\{l,m\}$,

$$(\mathbf{X}_{ii'})^{LL'}=X^{LL'}_{ii'}, \tag{13}$$

and defining a lattice-Fourier transformation

$$\mathbf{X}_{\mathbf{k}}=\frac{1}{N_s}\sum_{i,i'}e^{i\mathbf{k}\cdot(\mathbf{R}_i-\mathbf{R}_{i'})}\mathbf{X}_{ii'}, \tag{14}$$

where N_s is the number of lattice sites, we get Dyson's equation in the form

$$\mathbf{G}_{ii'\sigma}(E)=\frac{1}{N_s}\sum_{\mathbf{k}}\frac{e^{i\mathbf{k}\cdot(\mathbf{R}_i-\mathbf{R}_{i'})}}{(E+\mu)\mathbf{S}_{\mathbf{k}}-\mathbf{t}_{\mathbf{k}}-\mathbf{\Sigma}_{\mathbf{k}\sigma}(E)}. \tag{15}$$

Here the matrices $\mathbf{t}_{\mathbf{k}}$ and $\mathbf{S}_{\mathbf{k}}$ are the Fourier-transformed hopping and overlap integrals of Eqs. (2) and (3), respectively. $\mathbf{\Sigma}_{\mathbf{k}\sigma}(E)$ is the self-energy. The one-particle spectral density is given by

$$\mathbf{A}_{ii'\sigma}(E)=-\frac{1}{\pi}\mathrm{Im}\,\mathbf{G}_{ii'\sigma}(E+i0^+). \tag{16}$$

The on-site terms of the spectral density are diagonal in the orbital index as a consequence of lattice symmetries, and we have for the orbital-resolved QDOS

$$\rho^L_\sigma(E)=A^{LL}_{ii\sigma}(E-\mu), \tag{17}$$

where we dropped the site index. The total QDOS is obtained via

$$\rho_\sigma(E)=\sum_{i'}\mathrm{Tr}\{\mathbf{S}_{ii'}\mathbf{A}_{i'i\sigma}(E-\mu)\}. \tag{18}$$

To calculate the self-energy, we use a standard approximation scheme, the second-order perturbation theory around the Hartree-Fock solution[39–41,47,48] (SOPT-HF). It is known from the single-band Hubbard model that the nonlocal terms of the SOPT-HF self-energy rapidly decrease with increasing number of shells taken into account.[47,48] Furthermore, due to the band degeneracy, there is a much weaker **k** dependence of the SOPT-HF self-energy compared to the single-band case.[41] We may thus employ the local approximation

$$\Sigma^{LL'}_{ii'\sigma}(E)\approx\Sigma^{LL'}_{ii\sigma}(E)\,\delta_{ii'}=\Sigma^{L}_{\sigma}(E)\,\delta_{LL'}\delta_{ii'}. \tag{19}$$

As for the on-site Green function, lattice symmetries require the on-site self-energy to be diagonal in the orbital index.

The Hartree-Fock contribution to the self-energy reads as

$$\Sigma^{(\mathrm{HF}),L}_{\sigma}=\sum_{L_1}\{U_{LL_1LL_1}(n^{L_1}_{-\sigma}-n^{(0)L_1}_{-\sigma})+(U_{LL_1LL_1}-U_{LL_1L_1L})\times(n^{L_1}_{\sigma}-n^{(0)L_1}_{\sigma})\}, \tag{20}$$

where $n^L_\sigma=\langle n_{iL\sigma}\rangle$ denotes the expectation value in the full model and $n^{(0)L}_\sigma$ the expectation value of the band-structure calculation that stems from the double counting correction in Eq. (5). Approximating the self-energy by $\Sigma^{(\mathrm{HF}),L}_{\sigma}$ corresponds to the LDA+U approach.[44] Here we additionally include the next order in the interaction. The second-order contribution (SOC) to the self-energy reads as

$$\begin{aligned}\Sigma^{(\mathrm{SOC}),L}_{\sigma}(E)=&\int\int\int\frac{dx\,dy\,dz}{E-x+y-z}[f_-(x)f_-(-y)f_-(z)\\&+f_-(-x)f_-(y)f_-(-z)]\\&\times\sum_{L_1,L_2,L_3}U_{LL_1L_3L_2}\tilde{\rho}^{L_3}_{\sigma}(x)\\&\times\{U_{L_3L_2LL_1}\tilde{\rho}^{L_1}_{-\sigma}(y)\tilde{\rho}^{L_2}_{-\sigma}(z)+(U_{L_3L_2LL_1}\\&-U_{L_3L_2L_1L})\tilde{\rho}^{L_1}_{\sigma}(y)\tilde{\rho}^{L_2}_{\sigma}(z)\},\end{aligned} \tag{21}$$

with the Fermi function $f_-(E)=(e^{\beta E}+1)^{-1}$ and where the local HF spectral density $\tilde{\rho}^L_\sigma(E)=A^{(\mathrm{HF}),LL}_{ii\sigma}(E)$ is obtained by using the HF self-energy (20) in Eq. (15). The SOPT-HF self-energy

$$\mathbf{\Sigma}_\sigma(E)=\mathbf{\Sigma}^{(\mathrm{HF})}_\sigma+\mathbf{\Sigma}^{(\mathrm{SOC})}_\sigma(E) \tag{22}$$

determines the full Green function via Eq. (15).

B. Core-valence interaction

1. Valence-band Green function

Let us now focus on the core hole screening in the initial state for AES. The CV interaction and the presence of the core hole introduce an additional (Hartree-like) term

$$\Sigma^{(\mathrm{CV},e),L}_{i\sigma}=-\delta_{ii_c}U^c_L \tag{23}$$

to the valence-band self-energy which breaks the translational symmetry. This term represents the core-hole potential at the lattice site i_c where the core hole was created (the superscript ''e'' indicates averaging in the restricted Hilbert-space $\mathcal{H}^e$; see Sec. III). It is responsible for the screening. The valence-band self-energy in the presence of the core hole then reads as

$$\mathbf{\Sigma}^e_{i\sigma}(E)=\mathbf{\Sigma}^{(\mathrm{VV},e)}_{i\sigma}(E)+\mathbf{\Sigma}^{(\mathrm{CV},e)}_{i\sigma}. \tag{24}$$

$\mathbf{\Sigma}^{(\mathrm{VV},e)}_\sigma(E)$ incorporates the VV-correlation effects and has the same structure as the self-energy (22) for the translational invariant system. But in contrast to its translational invariant counterpart, $\mathbf{\Sigma}^{(\mathrm{VV},e)}_\sigma(E)$ is defined in terms of the Green functions in the presence of the core hole.

The valence-band Green function $\mathbf{G}^e_{ii'\sigma}(E)$ in the presence of the core hole can be obtained by using Dyson's equation in the form

$$\mathbf{G}^e_{ii'\sigma}(E)=\mathbf{G}_{ii'\sigma}(E)+\sum_j\mathbf{G}_{ij\sigma}(E)[\mathbf{\Sigma}^e_{j\sigma}(E)-\mathbf{\Sigma}_\sigma(E)]\times\mathbf{G}^e_{ji'\sigma}(E). \tag{25}$$

In general $\mathbf{\Sigma}^e_{i\sigma}(E)-\mathbf{\Sigma}_\sigma(E)\neq0$ for a certain number of shells around the core-hole site because the VV-correlation effects depend on the occupation numbers, which as a consequence of the screening locally differ from the translational invariant ones. In the following we assume complete screening, i.e., charge neutrality at the site i_c, which is reasonable especially for $3d$ transition metals because the screening time scale is small compared to the lifetime of the core hole.[27] This implies $\mathbf{\Sigma}^e_{i\sigma}(E)-\mathbf{\Sigma}_\sigma(E)$ to be small for all sites i except for $i=i_c$. Neglecting the terms for $i\neq i_c$ one can solve Eq. (25):

$$\mathbf{G}^e_{ii'\sigma}(E)=\mathbf{G}_{ii'\sigma}(E)+\mathbf{G}_{ii_c\sigma}(E)\{[\mathbf{\Sigma}^e_{i_c\sigma}(E)-\mathbf{\Sigma}_\sigma(E)]^{-1}-\mathbf{G}_{i_ci_c\sigma}(E)\}^{-1}\mathbf{G}_{i_ci'\sigma}(E). \tag{26}$$

For $i=i'=i_c$ one obtains the local screened Green function at the core-hole site:

$$\mathbf{G}^e_{i_ci_c\sigma}(E)=\frac{1}{\mathbf{G}^{-1}_{i_ci_c\sigma}(E)-[\mathbf{\Sigma}^e_{i_c\sigma}(E)-\mathbf{\Sigma}_\sigma(E)]}. \tag{27}$$

The assumption of complete screening will be utilized as a condition to fix the CV-interaction parameter, which is taken to be the same for *s*, *p*, and *d* orbitals ($U^c_L\equiv U_c$).

2. Core Green function

To take into account the CV interaction for the core Green function,

$$g_{i_c\sigma_c}(E)=\langle\langle b_{i_c\sigma_c};b^\dagger_{i_c\sigma_c}\rangle\rangle_E=\frac{1}{E+\mu-\epsilon_c-\Sigma^c_{i_c\sigma_c}(E)}, \tag{28}$$

one may calculate the core self-energy $\Sigma^c_{i_c\sigma_c}(E)$ using, e.g., the SOPT-HF in the same way as for the valence-band Green function. On the other hand, it is believed that the core states are influenced by other and presumably more important effects, such as lifetime effects.[3] In fact, the core spectral density obtained within SOPT-HF turns out to be dominated by a δ peak that is shifted by about 1 eV below $\epsilon_c-\mu$. This

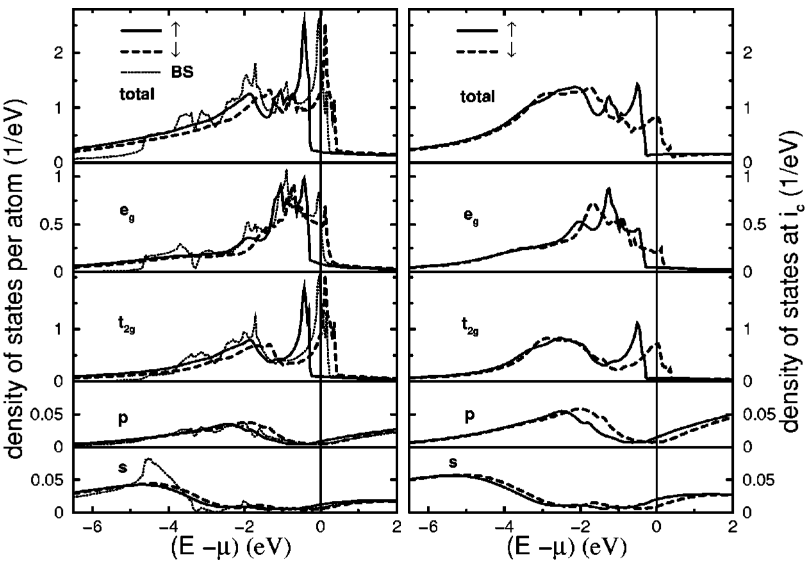

FIG. 1. Spin-resolved QDOS per atom for s, p, t_{2g}, and e_g states and total QDOS for $U=2.47$ eV, $J=0.5$ eV, and $T=0$ K. Left: unscreened QDOS. Thin dotted line: tight-binding band-structure calculation (Ref. 42) for paramagnetic Ni. Right: screened QDOS at the site i_c in the presence of the core hole, $U_c=1.81$ eV.

does not affect the Auger line shape. Therefore, we assume for convenience the core self-energy to be zero. The spectral density becomes

$$a_{i_c\sigma_c}(E)=-\frac{1}{\pi}\operatorname{Im} g_{i_c\sigma_c}(E+i0^+)=\delta(E+\mu-\epsilon_c). \tag{29}$$

C. Results for Ni

Before we discuss the results for fcc Ni, we like to make a short remark concerning the numerical evaluation of the theory. The **k** sum for the local Green function in Eq. (15) was performed on a mesh of 240 **k** points within the irreducible part of the Brillouin zone using the tetrahedron method[49] generalized to complex band structures, similar to that presented in Ref. 50. The evaluation of the total QDOS (18) as well as the QDOS in the presence of the core hole was done in **k** space. For the latter, Eq. (25) has to be used to perform the Fourier transformation.

The effective Slater integrals or, equivalently, the averaged direct and exchange interaction parameters are chosen as $U=2.47$ eV and $J=0.5$ eV. This leads to a calculated magnetic moment per atom of $m=0.56\mu_B$ at $T=0$ K which is the same as the measured moment.[51] With the ratio $J/U \approx 0.2$ we assume a typical value for the late $3d$ transition metals. The values given in the literature, for instance, $U=3.7$ eV, $J=0.27$ eV (Ref. 41) and $U=2.97$ eV, $J=0.8$ eV (Ref. 52) are of the same order of magnitude but slightly overestimate the magnetic moment within the present theory.

The ''free'' DOS, used as starting point for our theory, is shown on the left of Fig. 1 (thin dotted line) and corresponds to tight-binding band-structure calculations[42] for paramagnetic fcc Ni.

The left-hand side (LHS) of Fig. 1 shows the QDOS per atom for the model parameters given above. As is known from the experiment, Ni is a strong ferromagnet; i.e., the majority-spin states are fully occupied. The renormalization effects of the *a priori* uncorrelated s and p states seen in Fig. 1 can be traced back to the hybridization with the d states.

Taking into account the presence of the core hole and following the procedure to fix the CV interaction parameter as described above (charge neutrality) leads to $U_c=1.81$ eV. The corresponding ''screened'' QDOS is plotted on the right-hand side (RHS) of Fig. 1. The structure has changed remarkably. Spectral weight of the d electrons from the upper band edge is transferred to lower energies; the s and p states are more populated, too. The screened magnetic moment at the site i_c ($m^e_{i_c}=0.1\mu_B$ at $T=0$ K) is considerably decreased since the local occupation is increased (see also Fig. 3).

The left side of Fig. 2 shows the self-energy $\Sigma^L_\sigma(E)$. Within an energy range of about 1 eV above and below $E=0$ eV one has $\operatorname{Im}\Sigma^L_\sigma(E)\propto E^2$. Thus we have well-defined quasiparticles at the Fermi energy and their weight

$$z^L_\sigma=\left|1-\frac{\partial \operatorname{Re}\Sigma^L_\sigma(E=0)}{\partial E}\right|^{-1} \tag{30}$$

is 0.887 for the $t_{2g}\uparrow$ states and 0.893 for $t_{2g}\downarrow$ states. For e_g states we find 0.878 and 0.883, respectively. For energies above -2 eV, where one finds clearly distinguishable structures, a significant band narrowing caused by the real part of the self-energy is observed, while the imaginary part of the self-energy leads to strong damping effects in the QDOS (Fig. 1, LHS) for energies below -2 eV. About -6 eV

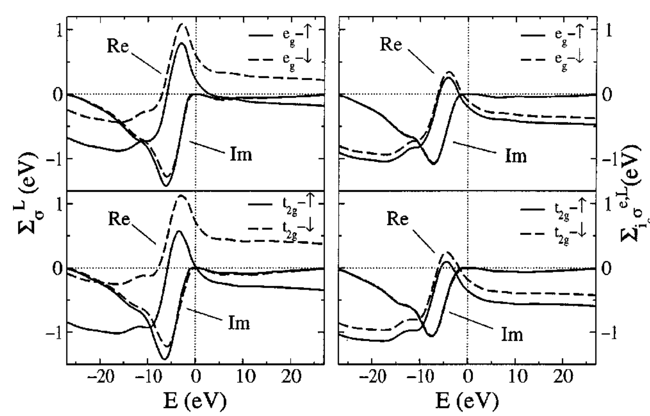

FIG. 2. Real and imaginary parts of the self-energy. Left: for the translationally invariant system $[\Sigma^L_\sigma(E)]$. Right: for the system in the presence of the core hole $[\Sigma^{eL}_{i_c\sigma}(E)]$.

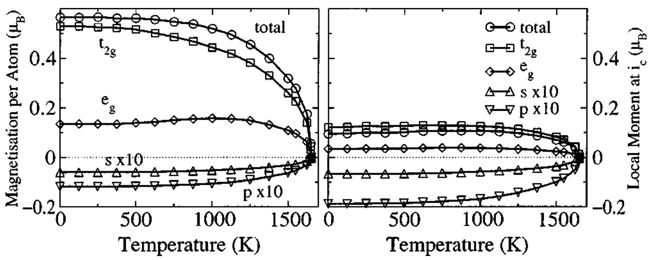

FIG. 3. Left: magnetization as a function of temperature. Right: local moment as a function of temperature in the presence of the core hole.

below the Fermi energy where one expects the ''Ni 6-eV satellite''[53–55] we find the largest damping effects. However, we do not find the correlation-induced 6 eV satellite. This is not surprising by applying the SOPT-HF or any other finite-order perturbational approach.[30,56,57] For different interaction parameters (larger U, smaller J) a small shoulder in the QDOS of the d states is visible as was also mentioned in Ref. 40.

On the right-hand side of Fig. 2 the self-energy in the presence of the core hole $\Sigma^{e,L}_{i_c\sigma}(E)$ is plotted. Again there are well-defined quasiparticles, but with an enhanced weight compared to the case where the core hole is absent ($z^{t_{2g}}_{i_c\uparrow}=0.940$, $z^{t_{2g}}_{i_c\downarrow}=0.934$, $z^{e_g}_{i_c\uparrow}=0.937$, $z^{e_g}_{i_c\downarrow}=0.936$.) The screened case behaves less correlated than the unscreened case since here one is closer to the limit of completely filled bands.

Finally, we show the local magnetic moment per atom as a function of temperature in Fig. 3. The magnetization curves (Fig. 3, LHS) have a Brillouin-function-like form, except for the e_g magnetization which shows up a maximum at $T\approx 1100$ K. This can be traced back to a transfer of charge carriers from the e_g orbitals to the t_{2g} orbitals with increasing temperature. Because Ni is a strong ferromagnet, the charge-carrier transfer leads to an increase of the e_g magnetization. Contrarily, the t_{2g} magnetization is decreased in addition to the usual temperature-induced depolarization. This leads to a temperature-dependent increase of the ratio $m_{e_g}/(m_{t_{2g}}+m_{e_g})$ as is known from polarized neutron-scattering experiments.[58,59] For $T=0$ K this ratio is 0.20 and in good agreement with the measured value of 0.19.[58,59] As is observed experimentally, the s and p states couple antiferromagnetically to the d states.[58,59] The Curie temperature turns out to be $T_C=1655$ K and is thereby about a factor of 2.6 larger than the measured value of 624 K.[60] The large value for T_C is probably due to the mean-field character of the SOPT-HF. Note, however, that a simple LDA+U (HF) calculation for the same parameters U and J yields a $T=0$ magnetization $0.57\mu_B$ and a Curie temperature of approximately 2500 K.

The local moment at the site i_c as function of temperature is shown on the right-hand side of Fig. 3. Its d contribution is strongly reduced compared to the unscreened case while the s and p moments are increased. The strong reduction of the total magnetic moment will influence the spin polarization of AES, since the ''screened'' QDOS enters the Auger Green function (10). Note that the total magnetization has to be calculated using Eq. (18), incorporating hybridization with delocalized states.

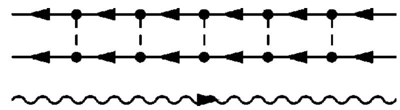

FIG. 4. Typical diagram of the VV ladder. Solid line: renormalized valence-band propagator. Wiggly line: core propagator. Dashed line: VV interaction.

V. DIRECT CORRELATIONS

To express the Auger intensity as a functional of the one-particle Green functions we consider the diagrammatic expansion of the three-particle Green function $G^{(3),\mathbf{LL}'}_{i_c\sigma\sigma_c}(E)$ [$\mathbf{L}=(L_1,L_2)$]. Here we can restrict ourselves to the direct diagrams and incorporate the exchange diagrams by introducing ''direct'' ($D^{\mathbf{L}}_{i_c\mathbf{k}}=M^{L_1L_2}_{i_c\mathbf{k}}$) and ''exchange'' Auger matrix elements ($E^{\mathbf{L}}_{i_c\mathbf{k}}=M^{L_2L_1}_{i_c\mathbf{k}}$). The Auger intensity then reads as

$$I_{\mathbf{k}\sigma\sigma_c}(E+\epsilon_c-\mu)\propto\delta(E-E(\mathbf{k}))\sum_{\mathbf{L},\mathbf{L}'}(\overline{D}^{\mathbf{L}}_{i_c\mathbf{k}}-\delta_{\sigma\sigma_c}\overline{E}^{\mathbf{L}}_{i_c\mathbf{k}})\times A^{(3),\mathbf{LL}'}_{i_c\sigma\sigma_c}(E)D^{\mathbf{L}'}_{i_c\mathbf{k}}. \tag{31}$$

The Auger matrix elements are taken to be constant. Following Ref. 12 we set

$$M^{L_1L_2}_{i_c\mathbf{k}}=\begin{cases}1 & \text{for } L_1\leqslant L_2,\\ -1 & \text{for } L_1>L_2.\end{cases} \tag{32}$$

We thereby account for the singlet contributions, i.e., the holes in the final state have opposite spin ($\sigma=-\sigma_c$), as well as for the triplet contributions ($\sigma=\sigma_c$) to the Auger intensity. The triplet contributions would be ignored if the Auger-matrix elements were chosen to be symmetric in the orbital index ($M^{L_1L_2}_{i_c\mathbf{k}}=M^{L_2L_1}_{i_c\mathbf{k}}$) because the transition operator then vanishes, as can be seen from Eq. (8).

A. VV ladder approximation

We consider two different approximation schemes for the treatment of the direct correlations. In the first approach, following Refs. 30–34 we neglect the direct CV correlations and treat the direct VV correlations by means of the VV ladder approximation, which becomes exact in the limit of completely filled or empty bands. A typical diagram contributing to the VV ladder is shown in Fig. 4. The solid lines represent the renormalized one-particle propagators of the valence band while the wiggly line is the one-particle core propagator. The dashed line corresponds to the VV interaction. Summing up all diagrams of this kind yields the VV ladder approximation. The three-particle spectral density is given by

$$A^{(3),\mathbf{LL}'}_{i_c\sigma\sigma_c}(E)=\int dE'A^{(2),\mathbf{LL}'}_{i_c\sigma\sigma_c}(E+E')a_{i_c\sigma_c}(E')f_+(E+E')\overset{(29)}{=}A^{(2),\mathbf{LL}'}_{i_c\sigma\sigma_c}(E+\epsilon_c-\mu)f_+(E+\epsilon_c-\mu), \tag{33}$$

where $f_+(E)=(e^{\beta E}-1)^{-1}$ is the Bose function. The two-particle valence-band spectral density $A^{(2),\mathbf{LL}'}_{i_c\sigma\sigma_c}(E)$ is ob-

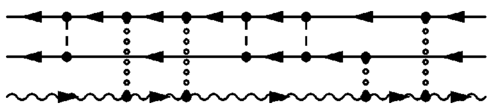

FIG. 5. Typical diagram in the CVV ladder approximation. The notation is the same as in Fig. 4. The additional CV interaction is represented by the dotted line.

tained from the corresponding two-particle Green function. Using a matrix notation with respect to $\mathbf{L}=\{L_1,L_2\}$ and $\mathbf{L}'$, the two-particle Green function reads as

$$\mathbf{G}^{(2)}_{i_c\sigma\sigma_c}(E)=\mathbf{G}^{(2,0)}_{i_c\sigma\sigma_c}(E)[1-\mathbf{U}\mathbf{G}^{(2,0)}_{i_c\sigma\sigma_c}(E)]^{-1}, \tag{34}$$

with $U_{\mathbf{LL}'}=U_{L_1L_2L_1'L_2'}$. $G^{(2,0),\mathbf{LL}'}_{i_c\sigma\sigma_c}(E)$ is the two-particle Green function that has to be calculated from the self-convolution of the partial QDOS,

$$A^{(2,0),\mathbf{LL}'}_{i_c\sigma\sigma_c}(E)=\delta_{\mathbf{LL}'}\int dE'\,\rho^{L_1}_{i_c\sigma}(E-E')\rho^{L_2}_{i_c\sigma_c}(E')$$
$$\times[f_-(E'-E)f_-(-E')$$
$$-f_-(E-E')f_-(E')], \tag{35}$$

using the spectral representation

$$G^{(2,0),\mathbf{LL}'}_{i_c\sigma\sigma_c}(E)=\int dE'\frac{A^{(2,0),\mathbf{LL}'}_{i_c\sigma\sigma_c}(E')}{E-E'}. \tag{36}$$

In Eq. (34) we have applied the local approximation; i.e., only the on-site elements for $i=i_c$ are assumed to be nonzero. This approximation is analogous to the local approximation for the one-particle Green function in Sec. IV.

B. VV and CV correlations

A straightforward way to include the direct CV correlation on the same level as the direct VV correlations has been discussed in Refs. 35–38. This leads to the (''three-particle'') CVV ladder approximation. For the limiting case of completely filled or empty bands the CVV ladder represents the exact solution and recovers the VV ladder but shifted energetically by $2U_c$ due to the CV interaction.[18] A typical diagram is shown in Fig. 5 where the dotted line represents the CV interaction. The CVV ladder approximation leads to a coupled set of Fredholm integral equations.[18] For a multiband model, however, the numerical evaluation is beyond our present computational capacities. We therefore discuss a simpler approximation where only diagrams up to first order in the direct correlations are retained (see Fig. 6).

C. Results for Ni

The calculated Auger spectra for Ni resulting from different approximations are shown in Fig. 7. The core hole is

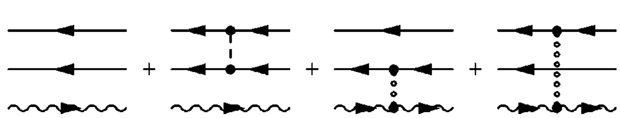

FIG. 6. Diagrams up to first order in the VV and CV interactions (notation as in Fig. 5).

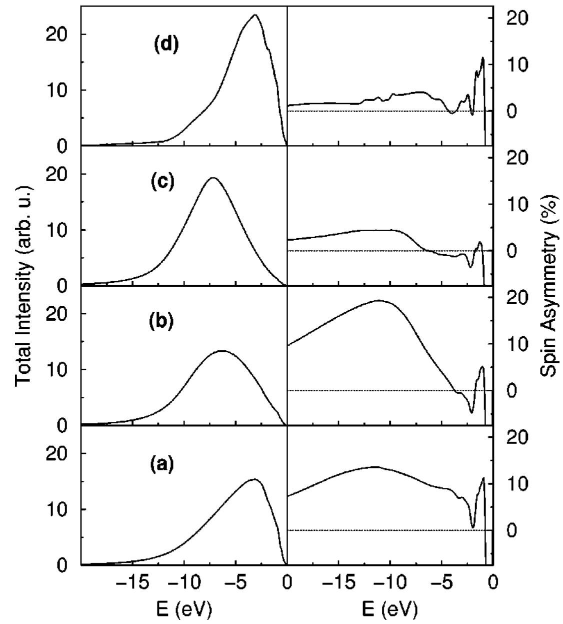

FIG. 7. Left: total intensities $I_\uparrow(E)+I_\downarrow(E)$. Right: spin asymmetry $[I_\uparrow(E)-I_\downarrow(E)]/[I_\uparrow(E)+I_\downarrow(E)]$. (a) Self-convolution without screening of the core hole in the initial state; (b) VV ladder without core hole screening; (c) screened VV ladder; (d) direct VV and CV correlations included up to first order (Fig. 6).

assumed to be unpolarized (nonresonant[61] process). The intensities for core spin σ_c and $-\sigma_c$ are added incoherently: $I_\sigma(E)=[I_{\sigma\sigma_c}(E)+I_{\sigma-\sigma_c}(E)]/2$. However, the Auger intensity is still spin dependent due to the ferromagnetic order in Ni. In Fig. 7 we plotted the total Auger intensity $I_\uparrow(E)+I_\downarrow(E)$ on the left and the spin asymmetry $[I_\uparrow(E)-I_\downarrow(E))/(I_\uparrow(E)+I_\downarrow(E)]$ on the right. Part (a) shows the result of the self-convolution model [Eqs. (33) and (35) inserted in Eq. (31)], i.e., the self-convolution of the occupied QDOS in Fig. 1 (LHS). Direct correlations and core-hole screening are neglected altogether. Part (b) corresponds to the VV ladder approximation starting from the (unscreened) QDOS. Taking additionally into account the screening effects introduced by the presence of the core hole in the initial state results in (c). The spectrum obtained by the first order in the direct VV and CV correlations (see Fig. 6) and by the screened QDOS is plotted in part (d).

As one can see in the plots on the left-hand side, the VV interaction is too weak to produce bound states, no sharp satellite appears, and the spectra appear to be bandlike. Compared to the self-convolution (a), however, a considerable shift to lower energies is observed in (b). This shift results from the direct correlations between the two final-state holes in the valence band. In (c) the main peak is shifted to still lower energies. This is an effect of the core-hole screening in the initial state and can be traced back to the redistribution of spectral weight in the screened QDOS (Fig. 1). Compared to (a) and (b), the total AES intensity is clearly increased in (c). Again this is a consequence of the core-hole screening since the number of occupied states available for the Auger process is increased (Fig. 1, RHS). The spectrum shown in (d) not only includes the initial-state core-hole screening but also the final-state effects due to the destruction of the core hole. Compared to (c), where the initial state is described in

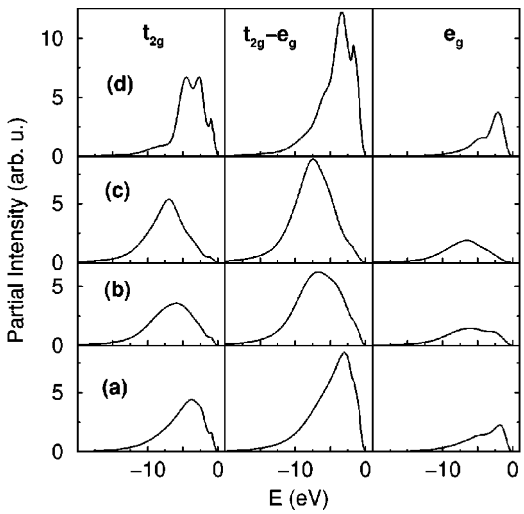

FIG. 8. Contributions to the total Auger intensity (Fig. 7) of processes involving t_{2g} electrons only (left), e_g electrons only (right), and both kinds of d electrons (middle).

the same way, these effects result in a strong shift of the main peak to higher energies. This shift almost exactly compensates for the shifts to lower energies that are due to direct VV correlations (b) and the core-hole screening (c). However, a weak shoulder at about $E=-8.5$ eV remains in the spectrum (d).

In all cases there is a high spin asymmetry (up to -50%) for energies between approximately -0.8 eV and 0. This is a consequence of the fact that Ni is a strong ferromagnet. There are almost no $\uparrow$ electrons above about -0.4 eV (see Fig. 1) that can participate in the Auger process. The main contribution to the intensity is therefore due to triplet configurations where the two final-state holes or, equivalently, core-hole and Auger electron have spin $\downarrow$. However, the intensity is very small in this energy region. By taking into account the screening of the core hole in the initial state [compare (b) and (c)] the spin asymmetry is reduced over the whole energy range which essentially is the same effect as the reduction of the local magnetic moment at i_c caused by the presence of the core hole (Fig. 3). The total spin-polarization

$$P=\frac{\int dEI_{\uparrow}(E)-\int dEI_{\downarrow}(E)}{\int dEI_{\uparrow}(E)+\int dEI_{\downarrow}(E)} \qquad (37)$$

in case (d) is 2.6% and 1.6% for (c). Both values are close to the experimental value[61] of 2% for the $M_1M_{45}M_{45}$ process. Cases (a) and (b) with a polarization of 8.7% and 9.3%, respectively, overestimate the total spin polarization compared with the experimental value.

For calculation of the orbitally resolved contributions to the Auger intensity we may restrict the summation in Eq. (31) to orbital indices (L_1,L_2,L_1',L_2') belonging to $t_{2g}(e_g)$ character only. The resulting contributions are shown on the left (right) of Fig. 8. The contributions due to the remaining $3d$ terms are plotted in the middle.

In all cases (a)–(d) the t_{2g} contributions are clearly stronger compared with the e_g contributions. The ratio between the t_{2g} and e_g partial intensities corresponds to the different degeneracies. Comparing the cases (a)–(d), we notice that there are essentially the same trends in the partial intensities as for the total intensities, and the discussion is the same as above. The line shape in case (d), however, shows up some fine structure, especially in the t_{2g} partial intensity, which is not that pronounced in the total intensity. The shoulder at the low-energy tail of (d) is due to direct VV correlations and may be interpreted as a hint at the formation of a bound state of the final holes. Except for this shoulder, a surprising similarity between (d) and (a) is noticed, even for the orbital-resolved spectra. This might also be due to the small number of diagrams taken into account. However, the cancellation of effects according to different interactions (VV and CV) was also pointed out in Ref. 27.

VI. SUMMARY

In this paper we have investigated electron-correlation effects on the Auger line shape of Ni as an example of a ferromagnetic $3d$ transition metal. The starting point is a realistic set of hopping and overlap parameters taken from tight-binding band-structure calculations. We additionally consider a strongly screened on-site Coulomb interaction between the rather localized $3d$ electrons. The respective Coulomb-matrix elements are expressed in terms of effective Slater integrals. Choosing a nonorthogonal basis, a distinction between the different angular momentum characters of the valence orbitals is possible. This is necessary for the precise definition of the Coulomb-interaction part in the (multiband Hubbard) Hamiltonian and also facilitates the interpretation of the Auger spectra. Furthermore, we account for the core-valence interaction which is responsible for the screening of the core hole in the initial state of AES and for the sudden response of the valence electrons due to the destruction of the core hole in the final state.

Within a diagrammatic approach, the indirect and the direct correlations can be studied separately. The indirect correlations have been treated by second-order perturbation theory around the Hartree-Fock solution (SOPT-HF). The VV interaction parameters are fixed by assuming a ratio $J/U\approx 0.2$ and by fitting the experimentally observed magnetic moment for $T=0$ K, leading to $U=2.47$ eV and $J=0.5$ eV. This is equivalent to an intraorbital interaction of $U_{LLLL}=3.04$ eV $(L=\{2,m_2\})$. The resulting Curie temperature within the theory presented here is by a factor of 2.6 larger than the experimentally observed one but considerably lower than the LDA$+U$ (Hartree-Fock) value.

The core-valence interaction leads to a breakdown of the translational invariance in the initial state for AES. The interaction parameter $U_c=1.81$ eV is fixed by requiring charge neutrality at the site i_c where the core hole is created. The screening of the additional core-hole potential causes a transfer of spectral weight below the Fermi energy and thus a considerable reduction of the local magnetic moment. However, the local magnetic moment is finite since the s and p electrons also contribute to the screening.

To study the direct correlations we have used two different approaches. The first is the VV ladder approximation, which results in a bandlike Auger spectrum with a single maximum. In a second approach we have summed up the first-order diagrams with respect to the VV and CV interactions. The resulting spectrum shows up a shoulder at the lower tail due to the VV interaction. Otherwise the line shape is very similar to that obtained by the self-convolution of the unscreened QDOS.

As far as concerns the line shape, we conclude that the different correlation effects, VV and CV correlations in the initial and the final state, nearly cancel. However, a strong effect of electron correlations has been found in the orbitally resolved partial intensities and particularly for the spin asymmetry.

The calculated spin polarization is in good agreement with the measured one of the $M_1M_{45}M_{45}$ process.[61] This process corresponds to the excitation of a not too deep lying core level, i.e., the two-step model should be applicable. The reduced but finite spin polarization of the $M_1M_{45}M_{45}$ process (as compared to the band polarization) can be explained by effects of core-hole screening rather than by a core-hole polarization, caused by a resonant excitation of the core electron into the valence band.[61] Future work will show whether these findings also apply to other $3d$ transition metals.

ACKNOWLEDGMENTS

Financial support of the Deutsche Forschungsgemeinschaft within the project No. 158/5-1 is greatfully acknowledged. The numerical calculations were performed on the CrayT3E at the Konrad-Zuse-Zentrum für Informationstechnik Berlin (ZIB).

APPENDIX: NONORTHOGONAL BASIS SET

There are several advantages for using the nonorthogonal basis set $\{|iL\sigma\rangle\}$. The Slater-Koster parameters[62] for the two-center approximation (used here) are much more accurate for a nonorthogonal basis set compared to an orthonormal one.[42] Second, the nonorthogonal basis [linear combination of atomic orbitals (LCAO) basis] is built up from quasiatomic orbitals. One therefore knows the behavior of the basis states under symmetry operations belonging to the O_h group which eventually results in the fact that local quantities, e.g., the on-site Green function, are diagonal in the orbital index. Furthermore, the Coulomb matrix elements can be calculated in a highly symmetric way by using $3j$ symbols in combination with a transformation from spheric to cubic harmonics. The unknown radial parts of the basis are parametrized by the effective Slater integrals (F^0,F^2,F^4). Finally, one can ensure that the Coulomb interaction acts between $3d$ electrons only.

For the formalism of second quantization, for the many-body and Green-function theory, for the proof of Wick's theorem and thus the development of the diagram technique, however, the use of an orthonormal set of one-particle basis states is necessary. Therefore, it is convenient to derive all expressions that refer to the nonorthogonal basis,

$$\langle\alpha|\beta\rangle = S_{\alpha\beta}, \tag{A1}$$

by a (nonunitary) Löwdin transformation[63] from a related set of orthogonal one-particle basis states:

$$|\tilde{\alpha}\rangle \overset{\text{Def}}{=} \sum_{\beta} |\beta\rangle S^{-1/2}_{\beta\alpha}. \tag{A2}$$

The overlap matrix $\mathbf{S}$ is Hermitian: $\{|\tilde{\alpha}\rangle\}$ indeed represents an orthonormal and complete basis set. The completeness relation can be written as

$$1 = \sum_{\alpha} |\tilde{\alpha}\rangle\langle\tilde{\alpha}| = \sum_{\alpha\beta\gamma} |\beta\rangle S^{-1/2}_{\beta\alpha} S^{-1/2}_{\alpha\gamma} \langle\gamma| = \sum_{\alpha\beta} |\alpha\rangle S^{-1}_{\alpha\beta}\langle\beta|. \tag{A3}$$

Annihilation (and creation) operators referring to the nonorthogonal basis may be defined as

$$c_\alpha \overset{\text{Def}}{=} \sum_{\beta} S^{-1/2}_{\alpha\beta}\tilde{c}_\beta. \tag{A4}$$

It is instructive to see how the creation operator acts on the vacuum state:

$$c^\dagger_\alpha|0\rangle = \sum_\beta \tilde{c}^\dagger_\beta S^{-1/2}_{\beta\alpha}|0\rangle = \sum_\beta |\tilde{\beta}\rangle S^{-1/2}_{\beta\alpha} = \sum_{\beta\gamma} |\gamma\rangle S^{-1/2}_{\gamma\beta} S^{-1/2}_{\beta\alpha}$$
$$= \sum_\beta |\beta\rangle S^{-1}_{\beta\alpha}. \tag{A5}$$

Furthermore, one gets from the transformations (A2) and (A4):

$$\sum_\alpha |\tilde{\alpha}\rangle\tilde{c}_\alpha = \sum_{\alpha\beta\gamma} |\beta\rangle S^{-1/2}_{\beta\alpha} S^{1/2}_{\alpha\gamma} c_\gamma = \sum_\alpha |\alpha\rangle c_\alpha. \tag{A6}$$

Thus, an operator in second quantization has the same structure for both the orthonormal and the nonorthogonal basis sets. A one-particle operator O, for example, reads as

$$O = \sum_{\alpha,\alpha'} \tilde{c}^\dagger_\alpha \langle\tilde{\alpha}|o|\tilde{\alpha}'\rangle \tilde{c}_{\alpha'} \overset{(A6)}{=} \sum_{\alpha,\alpha'} c^\dagger_\alpha \langle\alpha|o|\alpha'\rangle c_{\alpha'}. \tag{A7}$$

The nonorthogonal Green functions are defined as in the orthonormal case, e.g., $G_{\alpha\alpha'}(E) = \langle\langle c_\alpha ; c^\dagger_{\alpha'}\rangle\rangle$ for the one-particle Green function. For example, using the nonorthogonal version of the fundamental anticommutation rules ($[c_\alpha, c^\dagger_{\alpha'}]_+ = S^{-1}_{\alpha\alpha'}$; see also Eq. (4)) and the equation of motion, the noninteracting Green function turns out to be

$$\mathbf{G}^0(E) = [(E+\mu)\mathbf{S} - \mathbf{t}]^{-1}, \tag{A8}$$

where we used the matrix notation $(\mathbf{G})_{\alpha\alpha'} = G_{\alpha\alpha'}$, etc. For the interacting Green function one has [compare with Eq. (15)]

$$\mathbf{G}(E) = [(E+\mu)\mathbf{S} - \mathbf{t} - \mathbf{\Sigma}(E)]^{-1}. \tag{A9}$$

In the same way as for the examples given, one may use Wick's theorem, develop the diagram technique, etc.

*Electronic address: torsten.wegner@physik.hu-berlin.de

[1] J. C. Fuggle, *Electron Spectroscopy: Theory, Techniques and Applications* (Academic, London, 1981), Vol. 4, p. 85.
[2] R. Weissmann and K. Müller, Surf. Sci. Rep. **105**, 251 (1981).
[3] C.-O. Almbladh and L. Hedin, *Handbook on Synchrotron Radiation* (North-Holland, Amsterdam, 1983), Vol. 1b, p. 607.
[4] P. Weightman, *Electronic Properties of Surfaces* (Adam Hilger, Bristol, 1984), p. 135.
[5] S. B. Whitefield, G. B. Armen, R. Carr, J. C. Levin, and B. Crasemann, Phys. Rev. A **37**, 419 (1988).
[6] D. D. Sarma, C. Carbone, P. Sen, and W. Gudat, Phys. Rev. B **40**, 12 542 (1989).
[7] D. E. Ramaker, Crit. Rev. Solid State Mater. Sci. **17**, 211 (1991).
[8] D. D. Sarma, S. R. Barman, R. Cimino, C. Carbone, P. Sen, A. Roy, A. Chainani, and W. Gudat, Phys. Rev. B **48**, 6822 (1993).
[9] J. J. Lander, Phys. Rev. **91**, 1382 (1953).
[10] C. J. Powell, Phys. Rev. Lett. **30**, 1179 (1973).
[11] G. Hörmandinger, P. Weinberger, P. Marksteiner, and J. Redinger, Phys. Rev. B **38**, 1040 (1988).
[12] Y. Kucherenko and P. Rennert, J. Phys.: Condens. Matter **9**, 5003 (1997).
[13] M. Cini, Solid State Commun. **24**, 681 (1977).
[14] G. A. Sawatzky, Phys. Rev. Lett. **39**, 504 (1977).
[15] G. A. Sawatzky and A. Lenselink, Phys. Rev. B **21**, 1790 (1980).
[16] M. Cini, Phys. Rev. B **17**, 2788 (1978).
[17] W. Nolting, G. Geipel, and K. Ertl, Phys. Rev. B **45**, 5790 (1992).
[18] M. Potthoff, J. Braun, W. Nolting, and G. Borstel, J. Phys.: Condens. Matter **5**, 6879 (1993).
[19] W. Nolting, W. Borgiel, V. Dose, and T. Fauster, Phys. Rev. B **40**, 5015 (1989).
[20] W. Nolting, A. Vega, and T. Fauster, Z. Phys. B **96**, 357 (1995).
[21] M. Potthoff, T. Wegner, and W. Nolting, Phys. Rev. B **55**, 16132 (1997).
[22] H. Kajueter and G. Kotliar, Int. J. Mod. Phys. B **11**, 729 (1997).
[23] A. I. Lichtenstein and M. I. Katsnelson, Phys. Rev. B **57**, 6884 (1998).
[24] K. Held and D. Vollhardt, Eur. Phys. J. B **5**, 473 (1998).
[25] W. Metzner and D. Vollhardt, Phys. Rev. Lett. **62**, 324 (1989).
[26] M. I. Katsnelson and A. I. Lichtenstein, J. Phys.: Condens. Matter **11**, 1037 (1999).
[27] D. D. Sarma and P. Mahadevan, Phys. Rev. Lett. **81**, 1658 (1998).
[28] V. Drchal, J. Phys.: Condens. Matter **1**, 4773 (1989).
[29] M. Kotrla and V. Drchal, J. Phys.: Condens. Matter **4**, 4251 (1992).
[30] M. Cini, Surf. Sci. **87**, 483 (1979).
[31] G. Tréglia, M. C. Desjonquères, F. Ducastelle, and D. Spanjaard, J. Phys. C **14**, 4347 (1981).
[32] V. Drchal and J. Kudrnovský, J. Phys. F: Met. Phys. **14**, 2443 (1984).
[33] W. Nolting, Z. Phys. B: Condens. Matter **80**, 73 (1990).
[34] W. Nolting, G. Geipel, and K. Ertl, Phys. Rev. B **44**, 12 197 (1991).
[35] M. Potthoff, J. Braun, G. Borstel, and W. Nolting, Phys. Rev. B **47**, 12 480 (1993).
[36] M. Potthoff, J. Braun, and G. Borstel, Z. Phys. B **95**, 207 (1994).
[37] M. Potthoff, J. Braun, W. Nolting, and G. Borstel, Surf. Sci. **307-309**, 942 (1994).
[38] M. Potthoff, J. Braun, G. Borstel, and W. Nolting, J. Electron Spectrosc. Relat. Phenom. **72**, 163 (1995).
[39] A. A. Abrikosov, L. P. Gorkov, and I. E. Dzyaloshinski, *Methods of Quantum Field Theory in Statistical Mechanics* (Dover, New York, 1975).
[40] L. Kleinman and K. Mednick, Phys. Rev. B **24**, 6880 (1981).
[41] M. M. Steiner, R. C. Albers, and L. J. Sham, Phys. Rev. B **45**, 13 272 (1992).
[42] D. A. Papaconstantopoulos, *Handbook of the Band Structure of Elemental Solids* (Plenum, New York, 1986).
[43] S. Sugano, Y. Tanabe, and H. Kamimura, *Multiplets of Transition-Metal Ions in Crystals*, Vol. 33 of *Pure and Applied Physics* (Academic, New York, 1970).
[44] V. I. Anisimov, F. Aryasetiawan, and A. I. Lichtenstein, J. Phys.: Condens. Matter **9**, 767 (1997).
[45] D. N. Zubarev, Usp. Fiz. Nauk **71**, 71 (1961) [Sov. Phys. Usp. **3**, 320 (1960)].
[46] W. Nolting, *Vielteilchentheorie*, Vol. 7 of *Grundkurs: Theoretische Physik* (Zimmermann-Neufang, Ulmen, 1995).
[47] H. Schweitzer and G. Czycholl, Z. Phys. B **83**, 93 (1991).
[48] M. Potthoff and W. Nolting, Z. Phys. B **104**, 265 (1997).
[49] P. Lambin and J. P. Vigneron, Phys. Rev. B **29**, 3430 (1984).
[50] V. I. Anisimov, A. I. Poteryaev, M. A. Korotin, A. O. Anokhin, and G. Kotliar, J. Phys.: Condens. Matter **9**, 7359 (1997).
[51] S. Hirooka and M. Shimizu, Phys. Lett. **46A**, 209 (1973).
[52] M. Fleck, A. M. Oleś, and L. Hedin, Phys. Rev. B **56**, 3159 (1997).
[53] C. Guillot, Y. Ballu, J. Paigne, J. Lecante, K. P. Jain, P. Thiry, R. Pinchaux, Y. Petroff, and L. M. Falicov, Phys. Rev. Lett. **39**, 1632 (1977).
[54] Y. Sakisaki, T. Komeda, M. Ouchi, H. Kato, S. Masuda, and K. Yagi, Phys. Rev. Lett. **58**, 733 (1987).
[55] S. Raaen and V. Murgai, Phys. Rev. B **36**, 887 (1987).
[56] A. Liebsch, Phys. Rev. B **23**, 5203 (1981).
[57] V. Drchal, V. Janiš, and J. Kudranovský, cond-mat/9810181 (unpublished), http://xxx.lan.gov/abs/.
[58] P. J. Brown, J. Deportes, and K. R. A. Ziebeck, J. Phys. I **1**, 1529 (1991).
[59] P. J. Brown, J. Deportes, K. U. Neumann, and K. R. A. Ziebeck, J. Magn. Magn. Mater. **104-107**, 2083 (1992).
[60] M. B. Stearns, in *3d, 4d and 5d Elements, Alloys and Compounds*, edited by H. P. J. Wijn, Landoldt-Börnstein, New Series, Group III, Vol. 19, Pt. a (Springer, Berlin, 1984).
[61] R. Allenspach, D. Mauri, M. Taborelli, and M. Landolt, Phys. Rev. B **35**, 4801 (1987).
[62] J. C. Slater and G. F. Koster, Phys. Rev. **94**, 1498 (1954).
[63] P.-O. Löwdin, J. Chem. Phys. **18**, 365 (1950).